Supporting information for

High-performance donor-acceptor stenhouse adduct sensors with multi-stimuli response for efficient metal ion detection

Weixia Zhu, Youming Kou, Peixin Liu, Zhenya Wang, Haoran Wu*

School of Chemical Engineering, Zhengzhou University, Zhengzhou 450001, China

*Corresponding author: Haoran Wu

*Email: haoranwu@zzu.edu.cn

Table of Contents:

Section 1. Relevant literature on a chemical sensor for detecting Cu^{2+}, Fe^{3+}, and Al^{3+} ions.

Table S1. The E_T^N standard is based on the electronic transition of polar probe dyes in a series of solvents, which were chosen ten solvents and their corresponding E_T^N. The solvents are standardized into polar water (E_T^N=1.0) and non-polar tetramethylsilane (TMS) (E_T^N=0).[16, 17]

Solvent	DMSO	DMF	MeOH	AeCN	Ethanol
E_T^N	0.444	0.386	0.762	0.460	0.654
Solvent	Acetone	THF	Chloroform	DCM	Toluene
E_T^N	0.355	0.207	0.259	0.309	0.099

Table S2. The λ_{max} of L-D1 in different solvents.

Solvent	DMSO	DMF	MeOH	AeCN	Ethanol
λ_{max}	527 nm	526 nm	519 nm	526 nm	524 nm
Solvent	Acetone	THF	Chloroform	DCM	Toluene
λ_{max}	531 nm	539 nm	542 nm	540 nm	545 nm

Table S3. The λmax of L-D2 in different solvents.

Solvent	DMSO	DMF	MeOH	AeCN	Ethanol
λ_{max}	527 nm	527 nm	519 nm	525 nm	523 nm
Solvent	Acetone	THF	Chloroform	DCM	Toluene
λ_{max}	530 nm	539 nm	541 nm	539 nm	545 nm

Table S4. Relevant research on a dual chemical sensor for detecting Cu^{2+} and Fe^{3+} ions.

Sensor	Target	Detection Method	Solvent system	LOD(M)	Ref
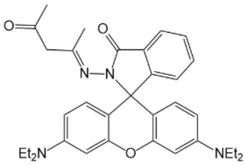	Cu^{2+}/Fe^{3+}	Fluorimetric	H_2O/Ethanol	Cu^{2+}: 4.8×10^{-8} Fe^{3+}: 3.9×10^{-9}	[1](2011)
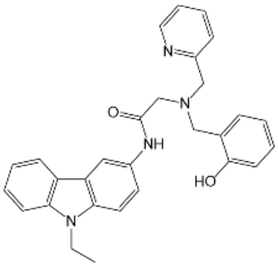	Cu^{2+}/Fe^{3+}	Colorimetric	DMF-buffer solution	Cu^{2+}: 2.9×10^{-6} Fe^{3+}: 1.35×10^{-7}	[2](2016)
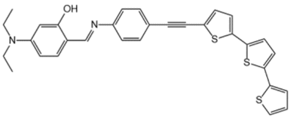	Cu^{2+}/Fe^{3+}	Fluorimetric Colorimetric	THF/ H_2O	Cu^{2+}: 4.48×10^{-7} Fe^{3+}: 1.09×10^{-7}	[3](2019)
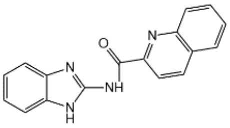	Cu^{2+}/Fe^{3+}	Fluorimetric	Tris-HCl buffer	Cu^{2+}: 1.35×10^{-7} Fe^{3+}: 1.24×10^{-7}	[4](2017)
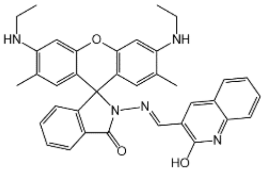	Cu^{2+}/Fe^{3+}	Fluorimetric	H_2O	Cu^{2+}: 1.8×10^{-8} Fe^{3+}: 3.3×10^{-8}	[5](2018)
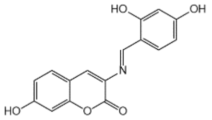	Cu^{2+}/Fe^{3+}	Fluorimetric	HEPES buffer /DMSO	Cu^{2+}: 1.04×10^{-4} Fe^{3+}: 4.87×10^{-5}	[6](2014)
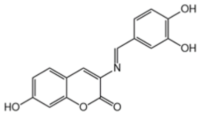	Cu^{2+}/Fe^{3+}	Fluorimetric	HEPES buffer /DMSO	Cu^{2+}: 1.27×10^{-4} Fe^{3+}: 5.17×10^{-5}	[6](2014)

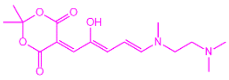

	Cu^{2+}/Fe^{3+}	Colorimetric	MeOH	Cu^{2+}: 6.6×10^{-8} Fe^{3+}: 1.1×10^{-7}	**This Work**
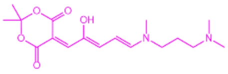	Cu^{2+}/Fe^{3+}	Colorimetric	MeOH	Cu^{2+}: 1.0×10^{-7} Fe^{3+}: 4.2×10^{-7}	**This Work**

Table S5. Relevant research on a chemical sensor for detecting Al^{3+} ions.

Sensor	**Target**	**Detection Method**	**Solvent system**	**LOD(M)**	**Ref**
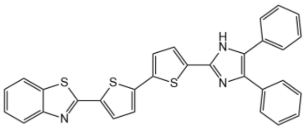	Al^{3+}	Fluorimetric	$AeCN/H_2O$	1.37×10^{-8}	[7](2023)
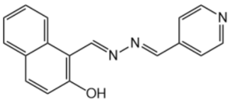	Al^{3+}	Fluorimetric	DMSO/HEPES buffer/H_2O	1.64×10^{-7}	[8](2023)
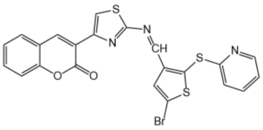	Al^{3+}	Fluorimetric	AeCN/PBS buffer	1.14×10^{-6}	[9](2021)
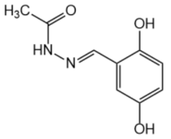	Al^{3+}	Fluorimetric	H_2O	6.6×10^{-7}	[10](2019)
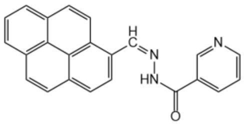	Al^{3+}	Fluorimetric	DMSO/ H_2O	1.7×10^{-7}	[11](2019)
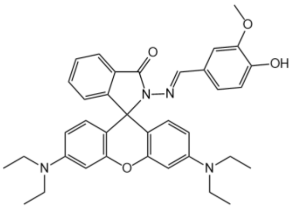	Al^{3+}	Fluorimetric Colorimetric	DMSO/MeOH	1.4×10^{-7}	[12](2015)
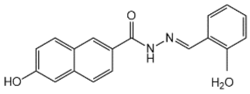	Al^{3+}	Fluorimetric	EtOH	3.02×10^{-7}	[13](2020)

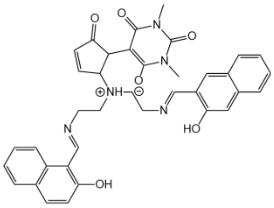	Al^{3+}	Fluorimetric Colorimetric	DMSO	3.65×10^{-7}	[14] (2022)
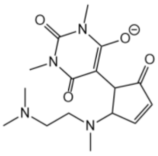	Al^{3+}	Colorimetric	MeOH	1.75×10^{-6}	[15] (2019)
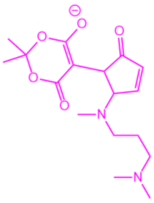	Al^{3+}	Colorimetric	MeOH	2.0×10^{-7}	**This work**

Section 2. Compounds Characterization

1. Synthesis of C-D1a

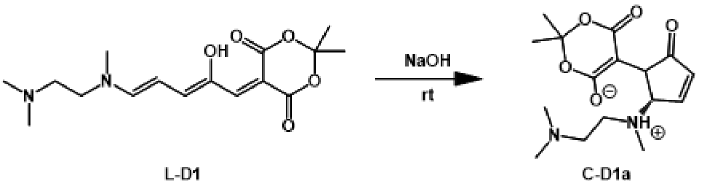

20 mg of L-D1 was taken and placed in a 5 mL centrifuge tube, followed by the addition of 0.5 mL of methanol and sonication to facilitate dissolution. Subsequently, 50 μL of sodium hydroxide methanol solution was added, resulting in a color change of the solution from deep red to brownish-yellow.

2. Synthesis of C-D1b

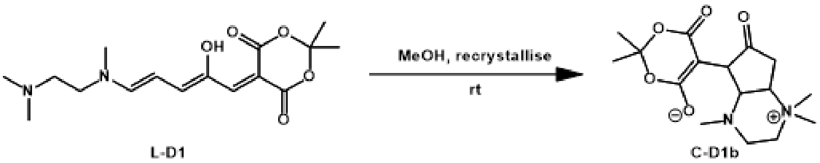

0.1 g of compound L-D1 was placed in a 20 mL sample bottle, followed by the addition of 5 mL of methanol and sonication until complete dissolution. Subsequently, 3 mL of anhydrous diethyl ether was slowly added to facilitate layering. The mixture was then left to stand in the dark for three days, resulting in the formation of 0.031 g of grayish-white crystalline solids, with a yield of 31%.

3. Synthesis of C-D2a

The synthesis of compound C-D2a was conducted following the method used for C-D1a.

4. ^{1}H NMR spectra, ^{13}C NMR spectra, FT-R and HRMS spectra

AFD: ^{1}H NMR (400 MHz, CDCl3) δ 8.48, 8.47, 8.36, 7.88, 7.87, 7.86, 6.77, 6.77, 6.77, 6.76, 6.76, 6.76, 6.76, 6.76, 1.78. ^{13}C NMR (101 MHz, $CDCl_3$) δ 163.25, 160.21, 150.49, 150.20, 141.21, 128.12, 115.31, 107.50, 104.52, 27.55.

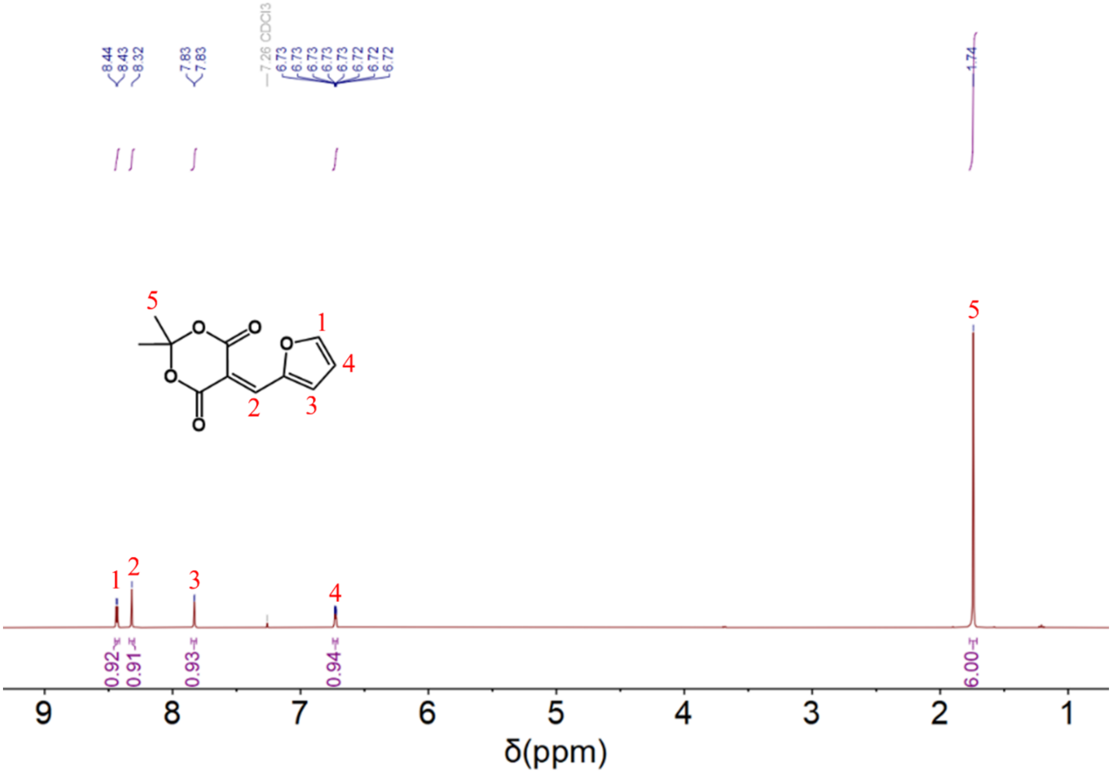

Fig S1. ^{1}H NMR Spectrum of **AFD** in $CDCl_3$ (400 MHz)

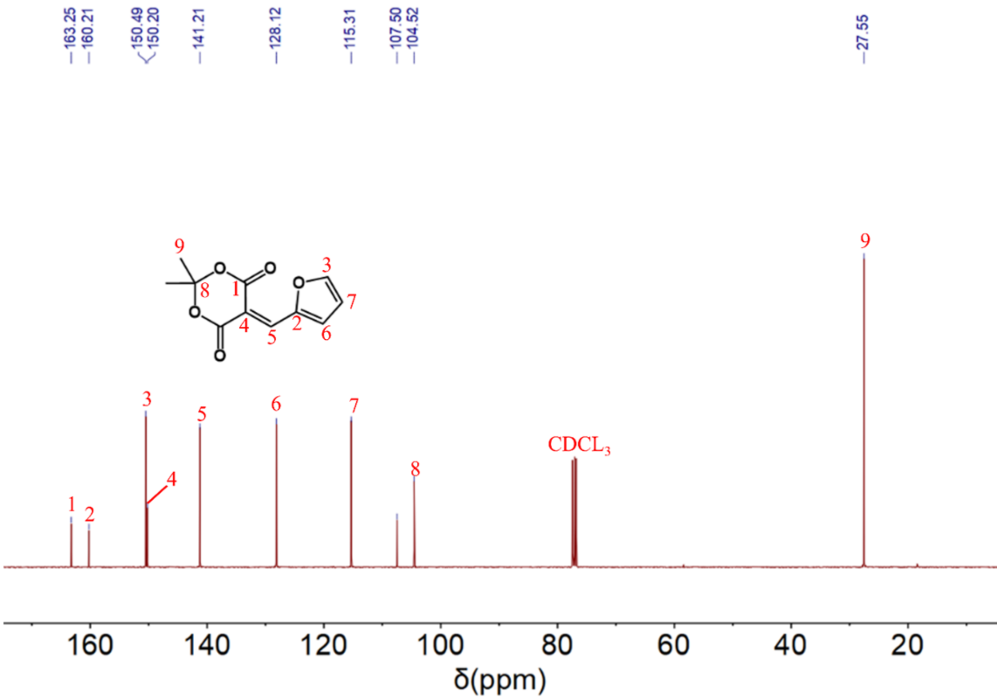

Fig S2. ^{13}C NMR Spectrum of **AFD** in CDCl$_3$ (101 MHz)

Fig S3. ^{1}H NMR spectrum of L-D1(DMSO-d6，400 MHz)

Fig S4. ^{1}H NMR spectrum of L-D2 (DMSO-d6，400 MHz)

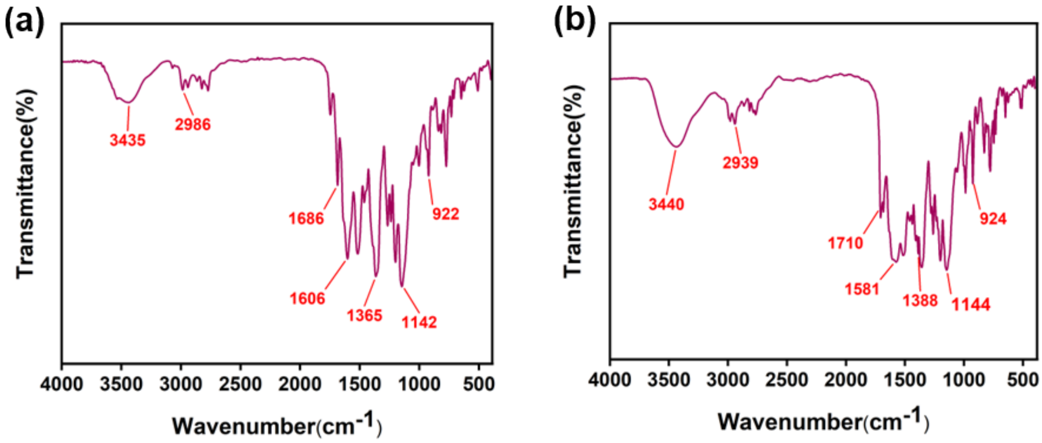

Fig S5. IR spectra of L-D1(a) and L-D2(b)

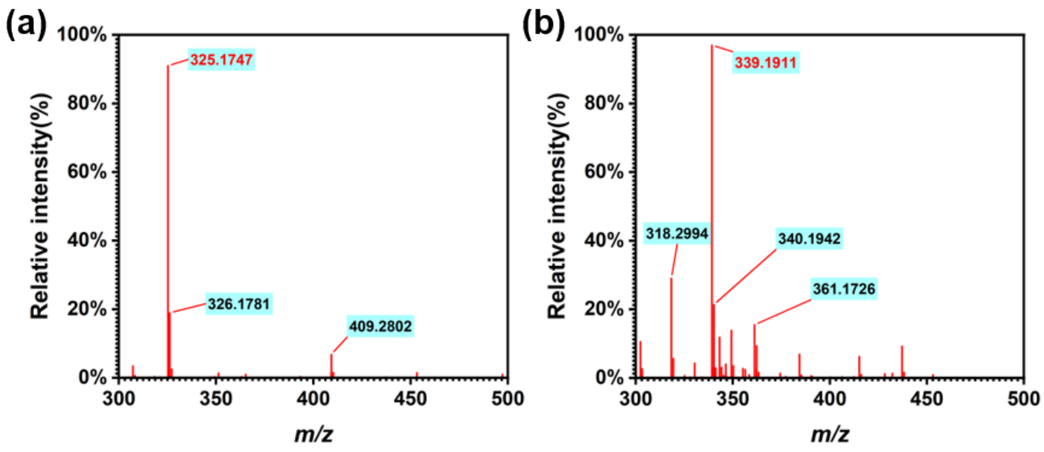

Fig S6. HRMS spectra of L-D1(a) and L-D2(b)

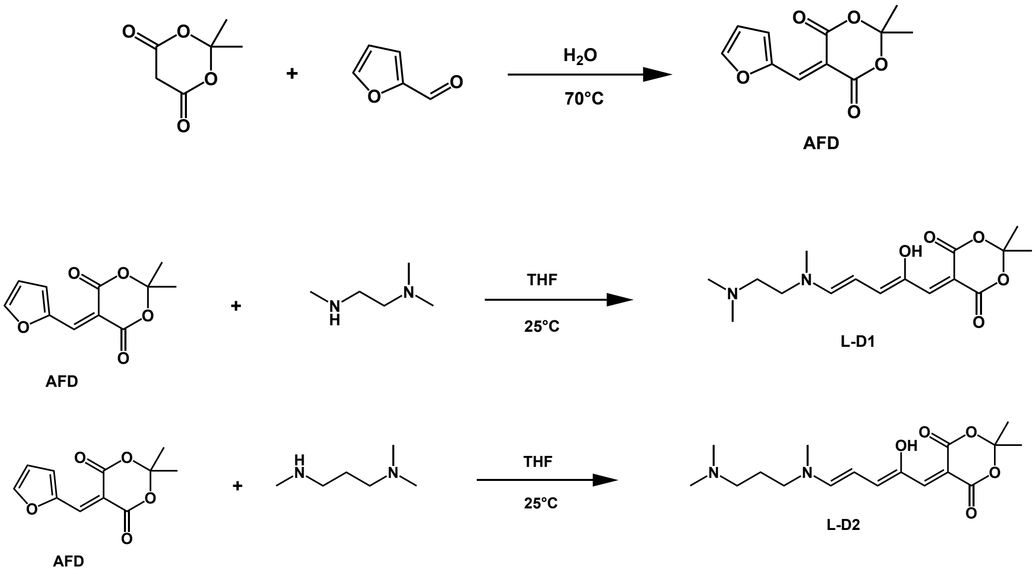

Scheme S1 Synthetic routes of L-D1 and L-D2

Section 3. The effect of solvents on L-D1 and L-D2

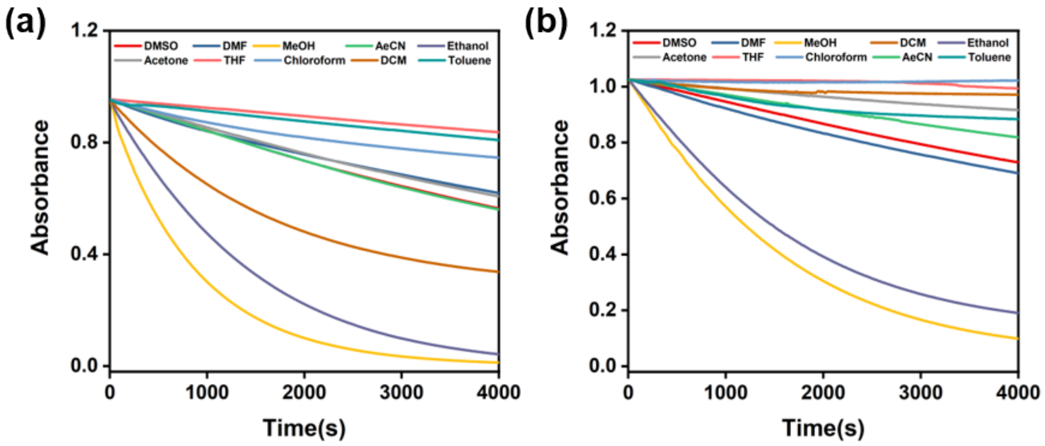

Fig S7. The normalized plot of the absorption values of L-D1(a) and L-D2(b) in different solvents as a function of time under dark conditions.

Section 4. Exploration of photoswitching and thermal recovery

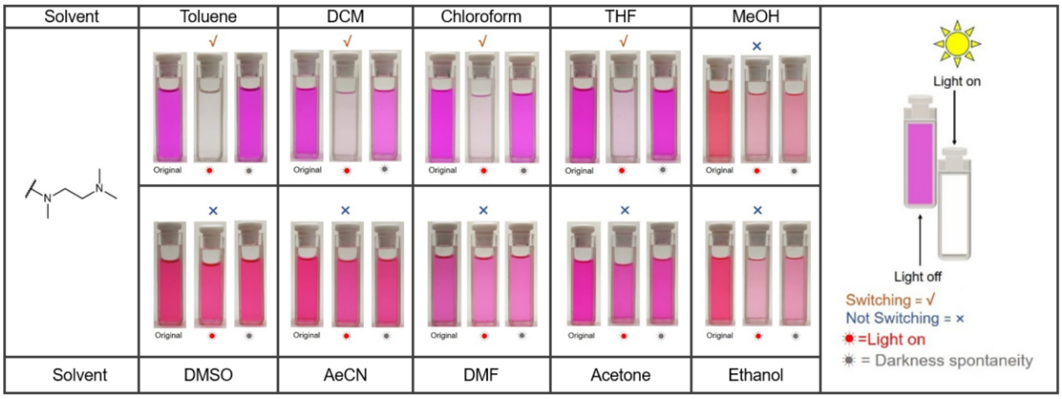

Fig S8. Comparison of the photoswitching ability of L-D1 in different solvents (irradiation time: 1h, 50µM, observed by naked eye colorimetry with potential errors).

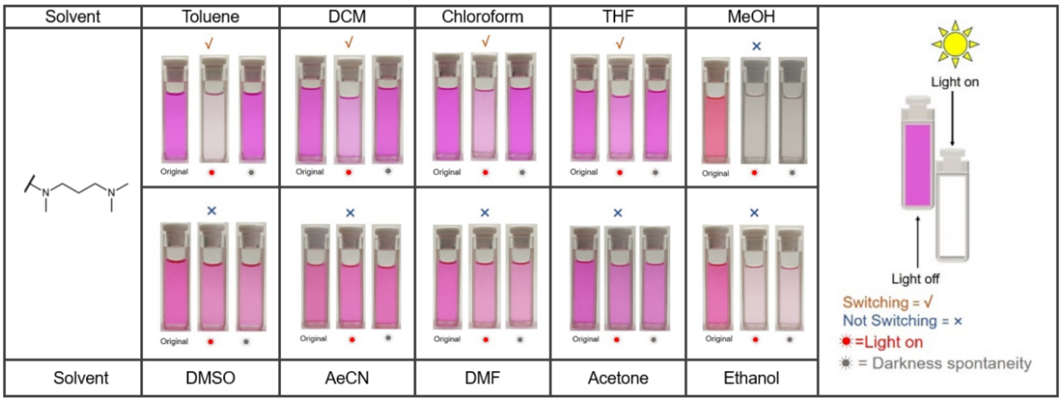

Fig S9. Comparison of the photoswitching ability of L-D2 in different solvents (irradiation time: 2 h, 20 μM, observed by naked eye colorimetry with potential errors).

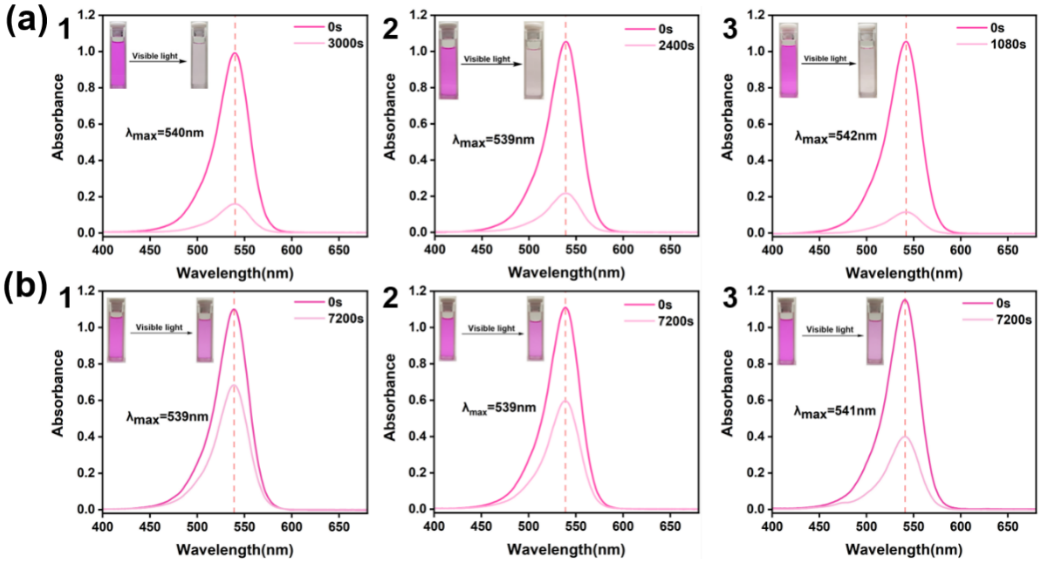

Fig S10. (a) UV-visible absorption spectra of the photo-induced isomerization process of L-D1 in dichloromethane, tetrahydrofuran, and chloroform. (b) UV-visible absorption spectra of the photo-induced isomerization process of L-D2 in dichloromethane, tetrahydrofuran, and chloroform. (1: DCM, 2: THF, 3: chloroform，20μM)

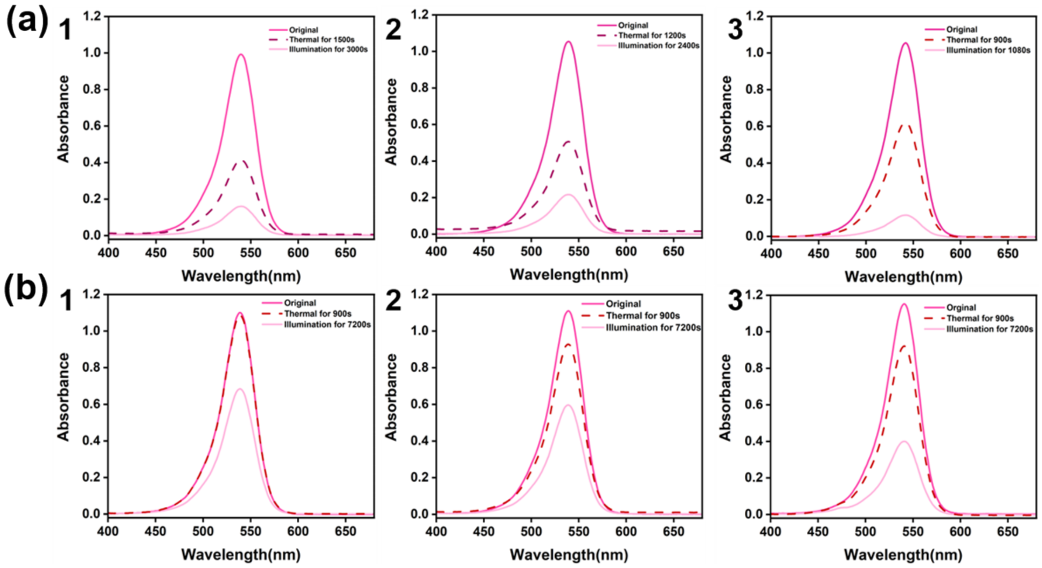

Fig S11. (a) UV-visible absorption spectra of the thermally-induced isomerization process of L-D1 in dichloromethane, tetrahydrofuran, and chloroform. (b) UV-visible absorption spectra of the thermally-induced isomerization process of L-D2 in dichloromethane, tetrahydrofuran, and chloroform. (1: DCM, 2: THF, 3: chloroform，20 μM)

Section 5. Kinetic discussion of the dark recovery process of L-D1 and L-D2 in toluene solvent[18-20].

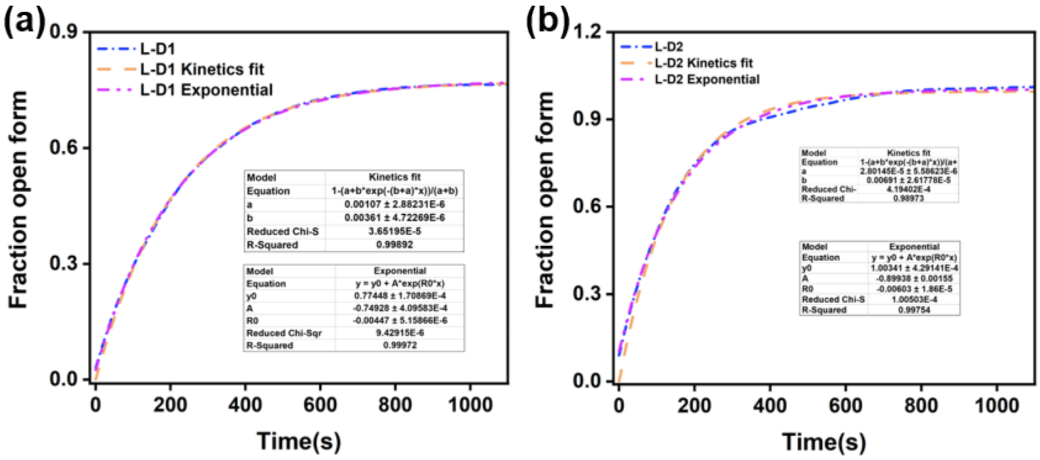

Fig S12. Kinetic fitting graph of the transformation from linear to cyclic structure of L-D1 (a) and L-D2 (b) in toluene under dark conditions. (20 μM)

$$\text{Open form} \underset{k_{-1}}{\overset{k_1}{\rightleftharpoons}} \text{Cyclic form}$$

The rates of opening and closing follow first-order kinetics, and the model can be represented as:

$$Equation.1\ y == 1 - \frac{k_1 + k_{-1}e^{-(k_1 + k_{-1})t}}{k_1 + k_{-1}}$$

The fitting of this process yields the following results:

L-D1: k: 10^{-3}; k_{-1}: 4×10^{-3} L-D2: k:3×10^{-5}; k_{-1}: 7×10^{-3}

In addition, the process of change conforms to the law of exponential functions:

$$Equation.2\ y = y_0 + Ae^{R_0 t}$$

(y: Content fractions of open ring structures; y_0: initial value; A: amplitude; R_0: rate constant; t: time(s))

Calculation of apparent half-life formula($t_{1/2}$):

$$Equation.3\ t_{\frac{1}{2}} = \frac{ln_{1/2}}{R_0}$$

Fitting the dark recovery process yields half-lives for L-D1 and L-D2:
L-D1: 155s，L-D2: 117s.

Section 6. Changes induced by acid-base stimulation

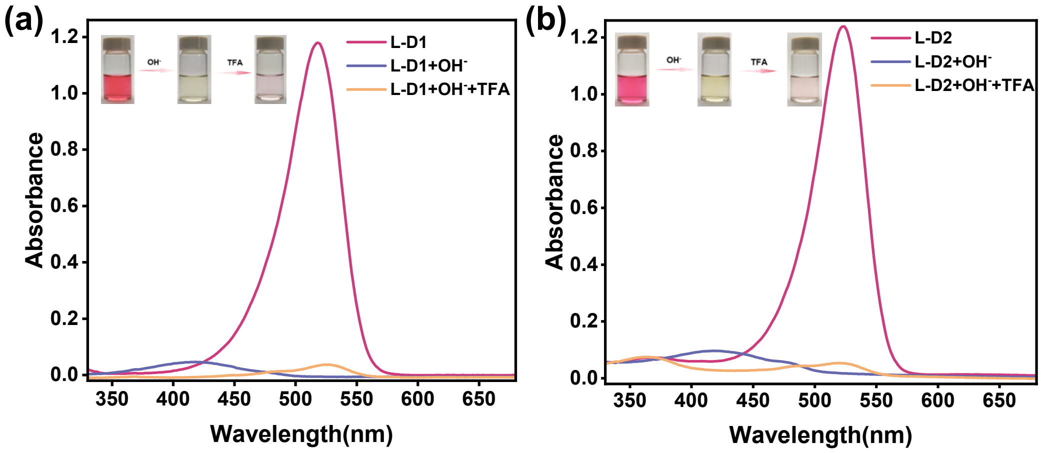

Fig S13. UV-Vis absorption spectra of L-D1 (a) and L-D2 (b) in response to the addition of OH^- in methanol solvent and cycling with trifluoroacetic acid.

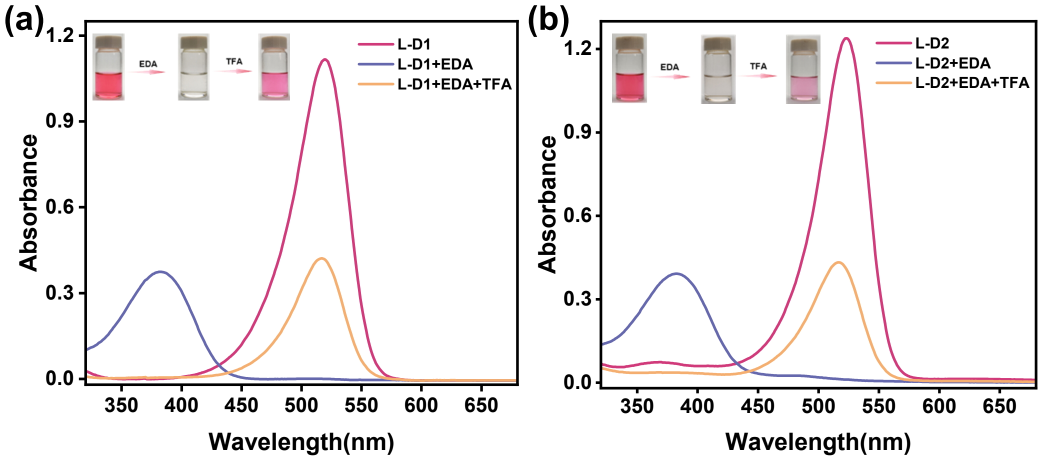

Fig S14. UV-Vis absorption spectra of L-D1 (a) and L-D2 (b) in response to cyclic addition of ethylenediamine and trifluoroacetic acid in methanol solvent.

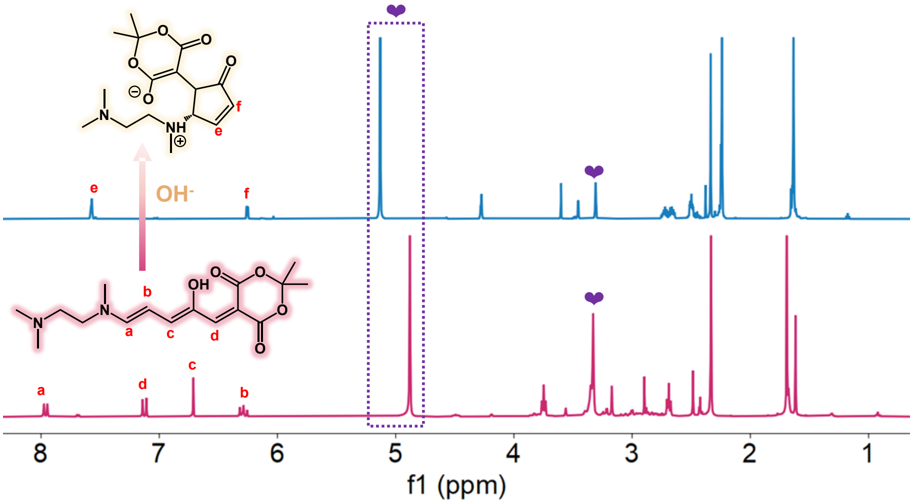

Fig S15. ^{1}H NMR comparison of L-D1 before and after OH$^-$ addition. (where the peaks labelled with hearts are solvent peaks)

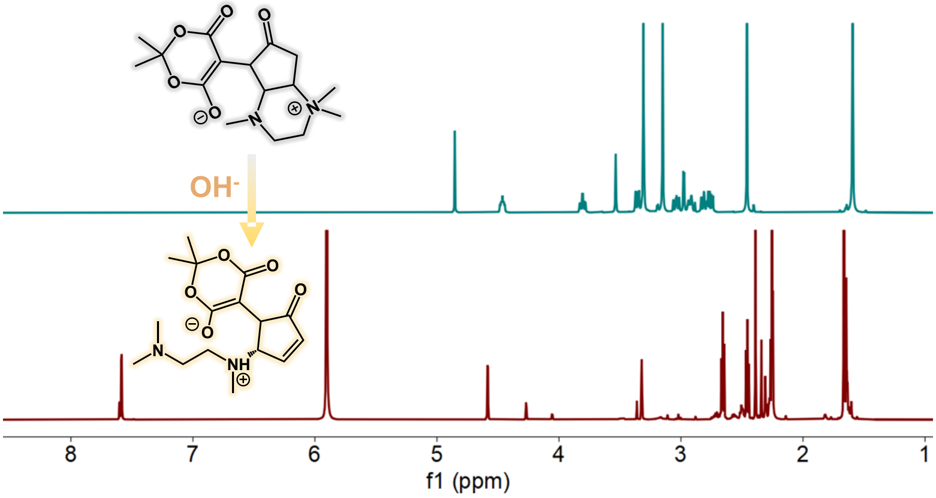

Fig S16. ^{1}H NMR comparison of C-D1b before and after base addition.

Section 7. Investigation of metal ion responsiveness

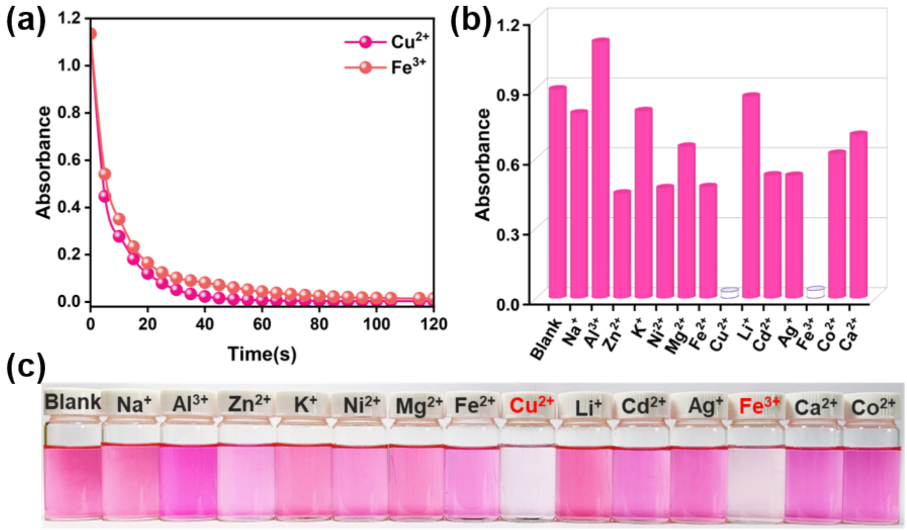

Fig S17. (a) Changes in absorbance over time in methanol solution of L-D2 upon addition of copper ions and iron ions (monitored at λ_{max} of 519 nm). (b) Comparison of absorbance intensity in methanol solution of L-D2 containing various metal ions (monitored at λ_{max} of 519 nm). (c) Colorimetric changes in methanol solution of L-D1 after the addition of various metal ions. (The concentrations of the metal ions are all

10^{-3} M, L-D2: 20 μM)

LOD（Limit of Detection）：

$$Equation.4\ LOD = \frac{3SD}{K}$$

where SD is the standard deviation of the blank sample, and K is the slope of the linear curve.

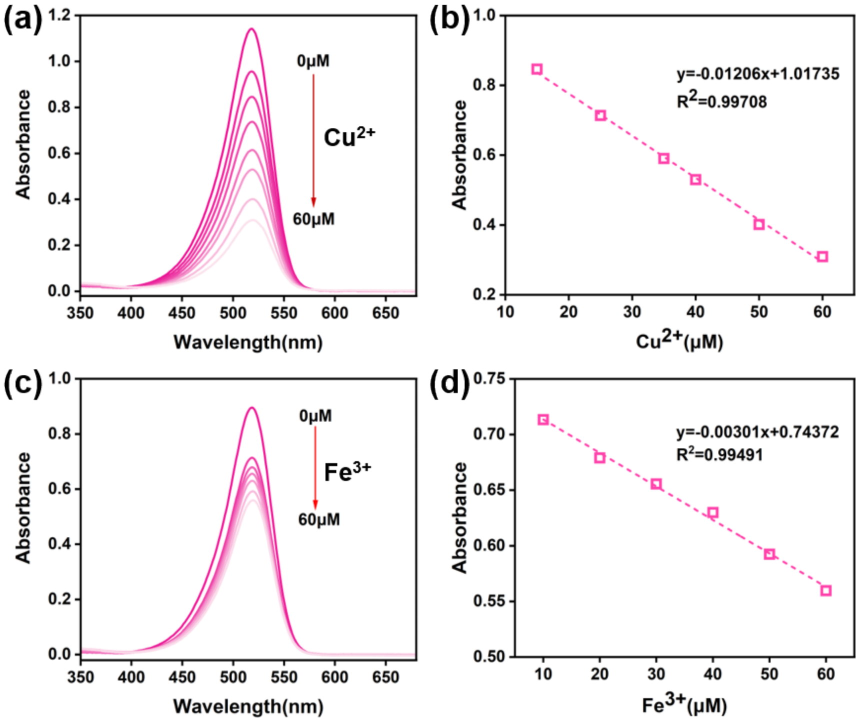

Fig S18. (a) Upon the addition of various amounts of copper ions, the UV-visible absorption spectra of L-D2 in methanol solutions were measured. (b) Upon the addition of various amounts of copper ions, the UV-visible absorption spectra of L-D2 in methanol solutions were measured. (c) Upon the addition of various amounts of iron ions, the UV-visible absorption spectra of L-D2 in methanol solutions were measured. (d) L-D2 detection limits for iron ions (monitored at λ_{max} of 519 nm).

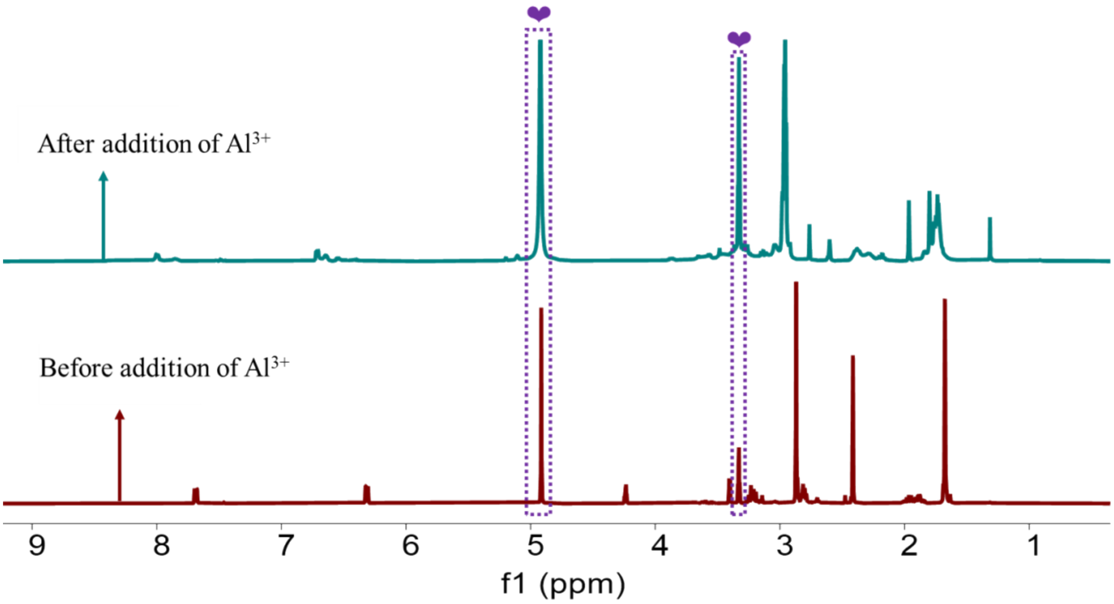

Fig S19. ^{1}H NMR comparison of C-D2a before and after addition of Al^{3+}. (where the peaks labelled with hearts are solvent peaks)

Section 8. References

References

[1] D. Zhong, Z. Cao, B. Wu, Q. Zhang and G. Wang, *Sens. Actuators B Chem.*, 2018, **254**, 385-392.

[2] G.J. Park, G.R. You, Y.W. Choi and C. Kim, *Sens. Actuators B Chem.,* 2016, **229**, 257-271.

[3] J. Wang, T. Wei, F. Ma, T. Li and Q. Niu, *J. Photochem. Photobiol. A*, 2019, **383**, 111982.

[4] B. Zhang, H. Liu, F. Wu, G. Hao, Y. Chen, C. Tan, Y. Tan and Y. Jiang, *Sens. Actuators B Chem.,* 2017, **243**, 765-774.

[5] A. Senthil Murugan, N. Vidhyalakshmi, U. Ramesh and J. Annaraj, *Sens. Actuators B Chem.,* 2018, **274**, 22-29.

[6] O. García-Beltrán, B. Cassels, C. Pérez, N. Mena, M. Núñez, N. Martínez, P.

Pavez and M. Aliaga, *Sensors*, 2014, **14**, 1358-1371.

[7] S.M. Kumar, S. Munusamy, S. Manickam, D. Jothi, S. Enbanathan and S.K. Iyer, *J. Mol. Liq.*, 2023, **381**, 121828.

[8] B. Musikavanhu, Z. Huang, Q. Ma, Y. Liang, Z. Xue, L. Feng and L. Zhao, *Spectrochim. Acta A Mol. Biomol. Spectrosc.*, 2023, **301**, 122961.

[9] B. Rani, A. Agarwala, D. Behera, V.P. Verma, A.P. Singh and R. Shrivastava, *Dyes Pigment.*, 2021, **194**, 109596.

[10] L. Wang, J. Yang, H. Wang, C. Ran, Y. Su and L. Zhao, *Sensors*, 2019, **19**, 2423.

[11] A. Saravanan, S. Shyamsivappan, T. Suresh, G. Subashini, K. Kadirvelu, N. Bhuvanesh, R. Nandhakumar and P.S. Mohan, *Talanta*, 2019, **198**, 249-256.

[12] V.K. Gupta, N. Mergu, L.K. Kumawat and A.K. Singh, *Talanta*, 2015, **144**, 80-89.

[13] X. Sun, T. Liu, N. Li, S. Zeng and Z. Xing, *Spectrochim. Acta A Mol. Biomol. Spectrosc.*, 2020, **228**, 117786.

[14] P. Fu, Q. Yan, S. Wang, H. Wu and D. Cao, *New J. Chem.*, 2022, **46**, 12600-12608.

[15] Y. Cai, T. Chen, X.Q. Chen and X. Bao, *Org. Lett.*, 2019, **21**, 7445-7449.

[16] M.M. Sroda, F. Stricker, J.A. Peterson, A. Bernal and J. Read De Alaniz, *Chem-Eur. J.,* 2021, **27**, 4183-4190.

[17] C. Reichardt, *Chem. Rev.*, 1994, **94**, 2319-2358.

[18] J.R. Hemmer, Z.A. Page, K.D. Clark, F. Stricker, N.D. Dolinski, C.J. Hawker and J. Read De Alaniz, *J. Am. Chem. Soc.*, 2018, **140**, 10425-10429.

[19] T.Y. Chen, Y.D. Cai, S.Q. Jiang, W. Cai, M.L. Tong and X. Bao, *ChemPhotoChem*, 2021, **5**, 559-564.

[20] M.M. Lerch, S.J. Wezenberg, W. Szymanski and B.L. Feringa, *J. Am. Chem.*

Soc., 2016, **138**, 6344-6347.